Inorganic Chemistry
Article

Inorg. Chem. **2009**, *48*, 11755–11766 **11755**
DOI: 10.1021/ic901826y

Influence of Bonding Mode of the Linkers in the Electronic Communication of Molecular Pairs Having Dimolybdenum Units Linked by Pseudohalides

F. Albert Cotton,† Carlos A. Murillo,* and Qinliang Zhao

Department of Chemistry, P.O. Box 3012, Texas A&M University, College Station, Texas 77842-3012.
†Deceased, February 20, 2007.

Received September 14, 2009

Depending on conditions the reactions of $[Mo_2(cis\text{-}DAniF)_2(NCCH_3)_4](BF_4)_2$ (DAniF = *N,N'*-di-*p*-anisylformamidinate) with solutions containing thiocyanate anions lead to two compounds: a quadruple-bonded dinuclear species **1**, $(Bu^n_4N)_2[Mo_2(cis\text{-}DAniF)_2(NCS)_4]$, and a molecular pair **3**, $[Mo_2(cis\text{-}DAniF)_2]_2(\mu_{1,3}\text{-}NCS)_4$. The latter has a cuboidal structure having two $(cis\text{-}DAniF)_2Mo_2^{2+}$ units, $[Mo_2]$, with four thiocyanate groups bridging two $[Mo_2]$ units in an end-to-end fashion in which the N and S atoms serve as the bridging units. On the contrary, the structure of the cyanate isomer, $[Mo_2(cis\text{-}DAniF)_2]_2(\mu_{1,1}\text{-}NCO)_4$ (**2**), shows an end-on binding of the cyanate linkers. Various physical measurements of **2** and its oxidized species $\mathbf{2}\cdot PF_6$ indicate that there is strong electronic communication between the two dimetal cores. For **1**, two reversible oxidation processes were observed in the cyclic voltammogram corresponding to the successive oxidation to $\mathbf{1}^+$ and an uncommon $\mathbf{1}^{2+}$ species that has a triple-bonded Mo_2^{6+} core. DFT calculations indicate that the antibonding character between the Mo−Mo δ orbitals and thiocyanate p orbitals plays a very important role in elevating the HOMO δ orbital energy that allows formation of the dication. A selenium isomer of **3** was also studied. In both the thiocyanate and selenocyanate bridged *dimers of dimers*, in which the pseudohalide bridges bind the two dimetal units in an end-to-end fashion, long separations between the dimetal units are observed, and these generate very weak electronic interactions.

Introduction

Electronic communication between two mononuclear species joined by a linker has been a topic of great importance and interest for quite a while. The earliest studies were done on species such as the Creutz−Taube ion (**I** in Scheme 1), a pyrazine-bridged diruthenium complex synthesized in the late 1960s;[1] a host of other such systems have since been investigated.[2] It is generally understood[3,4] that electronic interaction between two adjacent metal centers depends on diverse variables including geometric and bonding factors such as electrostatic interactions and electron delocalization (conjugation) through the linker.[5] Such studies have implications in a range of interdisciplinary areas for reasons that vary from augmenting fundamental chemistry knowledge, to a better understanding of important biochemical redox and electron transfer processes,[6] to fabrication of nanoscale structures in materials science.[7]

Scheme 1

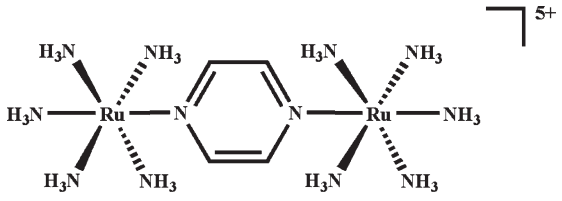

I

*To whom correspondence should be addressed. E-mail: murillo@tamu.edu.

(1) (a) Creutz, C.; Taube, H. *J. Am. Chem. Soc.* **1969**, *91*, 3988. (b) Creutz, C.; Taube, H. *J. Am. Chem. Soc.* **1973**, *95*, 1086.

(2) See, for example: (a) Creutz, C. *Prog. Inorg. Chem.* **1983**, *30*, 1. (b) Richardson, D. E.; Taube, H. *Coord. Chem. Rev.* **1984**, *60*, 107. (c) Dogan, A.; Sarkar, B.; Klein, A.; Lissner, F.; Schleid, T.; Fiedler, J.; Zalis, S.; Jain, V. K.; Kaim, W. *Inorg. Chem.* **2004**, *43*, 5973. (d) Chisholm, M. H.; Feil, F.; Hadad, C. M.; Patmore, N. J. *J. Am. Chem. Soc.* **2005**, *127*, 18150. (e) Rigaut, S.; Olivier, C.; Costuas, K.; Choua, S.; Fadhel, O.; Massue, J.; Turek, P.; Saillard, J.-Y.; Dixneuf, P. H.; Touchard, D. *J. Am. Chem. Soc.* **2006**, *128*, 5859. (f) D'Alessandro, D. M.; Dinolfo, P. H.; Davies, M. S.; Hupp, J. T.; Keene, F. R. *Inorg. Chem.* **2006**, *45*, 3261.

(3) (a) Crutchley, R. J. *Adv. Inorg. Chem.* **1994**, *41*, 273. (b) Kaim, W.; Klein, A.; Glöckle, M. *Acc. Chem. Res.* **2000**, *33*, 755.

(4) (a) Creager, S.; Yu, C. J.; Bamdad, C.; O'Connor, S.; MacLean, T.; Lam, E.; Chong, Y.; Olsen, G. T.; Luo, J.; Gozin, M.; Kayyem, J. F. *J. Am. Chem. Soc.* **1999**, *121*, 1059. (b) Launary, J.-P. *Chem. Soc. Rev.* **2001**, *30*, 386.

(5) Demadis, K. D.; Harshorn, M.; Meyer, T. J. *Chem. Rev.* **2001**, *101*, 2655.

(6) See, for example: (a) Prassides, K. *Mixed-valency Systems. Applications in Chemistry, Physics and Biology*; Kluwer Academic Publishers: Dordrecht, The Netherlands, 1991. (b) Blondin, G.; Gired, J.-J. *Chem. Rev.* **1990**, *90*, 1359 and references therein. (c) Gamelin, D. R.; Bominaar, E. L.; Kirk, M. L.; Wieghardt, K.; Solomon, E. I. *J. Am. Chem. Soc.* **1996**, *118*, 8085 and references therein.

Published on Web 11/02/2009

Scheme 2

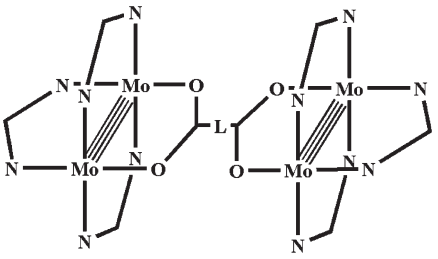

II (L = dicarboxylate)

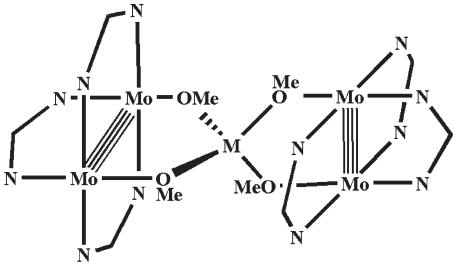

III (M = Zn, Co)

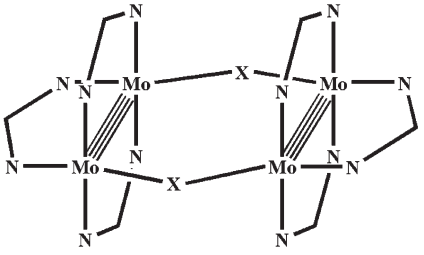

IV (X = H, OH)

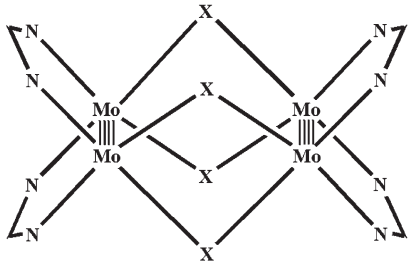

V (X = Cl, Br, I and OR)

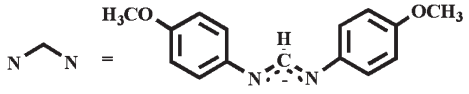

= *N*, *N*'-di(*p*-anisyl)formamidinate (DAniF)

Our group has devoted much attention to the study of compounds with quadruply bonded dimolybdenum subunits, $[Mo_2(DAniF)_n]^{(4-n)+}$ (n = 2 or 3, and DAniF = *N*,*N*′-di-*p*-anisylformamidinate) instead of single metal units, linked by various linkers.[5,8] For simplicity, such dimolybdenum units will be represented as $[Mo_2]$. By careful selection of the linkers and reaction conditions, compounds with a great variety of conformations and binding patterns such as those shown in Scheme 2 have been observed. This diversity has allowed better understanding of the effect of the linker on the electronic interactions between dimetal units. For instance, a tetrahedral inorganic linker, for example, $M(OCH_3)_4^{2-}$ (M = Zn or Co) (**III**), brings together two $[Mo_2]$ units in orthogonal directions, which severely limits electron delocalization over the two dimetal centers by hampering metal-to-ligand π-orbital-interaction pathways.[8j] When single atoms such as halogen groups serve as bridges, strong electronic coupling in the cuboidal tetranuclear compounds $[Mo_2(cis\text{-}DAniF)_2]_2(\mu\text{-}X)_4$ (**V**), X = Cl, Br, and I, has primarily been attributed to direct overlap between the δ orbitals from adjacent dimetal units.[9]

A common first approach to estimate electronic communication in a species having two metal-based centers is the use of electrochemical measurement to determine the potential difference between consecutive redox processes, $\Delta E_{1/2}$.[2b,c,10] The basic principle is based on the fact that, when an electron is removed from a metal-containing unit joined to another analogous unit by a linker, and then this process is followed by another oxidation process, the second metal unit will experience the positive charge in the neighboring unit in a different way that depends on how well or how poorly the linker allows charge delocalization. As a consequence for a linker that disfavors electronic communication, the potential for the removal of a second electron is not going to be significantly different from that of the first oxidation, and thus the $\Delta E_{1/2}$ will be small. On the contrary, a larger $\Delta E_{1/2}$ value is expected for a system having a linker that favors

(7) (a) Ward, M. D. *Chem. Soc. Rev.* **1995**, *34*, 121. (b) Astruc, D. *Acc. Chem. Res.* **1997**, *30*, 383. (c) McCleverty, J. A.; Ward, M. D. *Acc. Chem. Res.* **1998**, *31*, 842.

(8) (a) Cotton, F. A.; Donahue, J. P.; Lin, C.; Murillo, C. A. *Inorg. Chem.* **2001**, *40*, 1234. (b) Cotton, F. A.; Donahue, J. P.; Murillo, C. A. *J. Am. Chem. Soc.* **2003**, *125*, 5436. (c) Cotton, F. A.; Donahue, J. P.; Murillo, C. A. *Inorg. Chem.* **2001**, *40*, 2229. (d) Cotton, F. A.; Liu, C. Y.; Murillo, C. A.; Wang, X. *Inorg. Chem.* **2003**, *42*, 4619. (e) Cotton, F. A.; Daniels, L. M.; Donahue, J. P.; Liu, C. Y.; Murillo, C. A. *Inorg. Chem.* **2002**, *41*, 1354. (f) Cotton, F. A.; Liu, C. Y.; Murillo, C. A.; Villagrán, D.; Wang, X. *J. Am. Chem. Soc.* **2003**, *125*, 13564. (g) Cotton, F. A.; Liu, C. Y.; Murillo, C. A.; Villagrán, D.; Wang, X. *J. Am. Chem. Soc.* **2004**, *126*, 14822. (h) Cotton, F. A.; Donahue, J. P.; Murillo, C. A. *Inorg. Chem.* **2001**, *40*, 2229. (i) Cotton, F. A.; Liu, C. Y.; Murillo, C. A.; Wang, X. *Inorg. Chem.* **2003**, *42*, 4619. (j) Cotton, F. A.; Dalal, N. S.; Liu, C. Y.; Murillo, C. A.; North, J. M.; Wang, X. *J. Am. Chem. Soc.* **2003**, *125*, 12945. (k) Cotton, F. A.; Daniels, L. M.; Jordan, G. T., IV; Lin, C.; Murillo, C. A. *J. Am. Chem. Soc.* **1998**, *120*, 3398.

(9) (a) Cotton, F. A.; Liu, C. Y.; Murillo, C. A.; Wang, X. *Chem. Commun.* **2003**, 2190. (b) Cotton, F. A.; Liu, C. Y.; Murillo, C. A.; Zhao, Q. *Inorg. Chem.* **2006**, *45*, 9493.

(10) Joshi, H. K.; Cooney, J. J. A.; Inscore, F. E.; Gruhn, N. E.; Lichtenberger, D. L.; Enemark, J. H. *Proc. Natl. Acad. Sci. U. S. A.* **2003**, *100*, 3719.

(11) See, for example: (a) Ketterle, M.; Fiedler, J.; Kaim, W. *Chem. Commun.* **1998**, 1701. (b) Flanagan, J. B.; Margel, S.; Bard, A. J.; Anson, F. C. *J. Am. Chem. Soc.* **1978**, *100*, 4248. (c) Ito, T.; Hamaguchi, T.; Nagino, H.; Yamaguchi, T.; Kido, H.; Zavarine, I. S.; Richmond, T.; Washington, J.; Kubiak, C. P. *J. Am. Chem. Soc.* **1999**, *121*, 4625.

Scheme 3

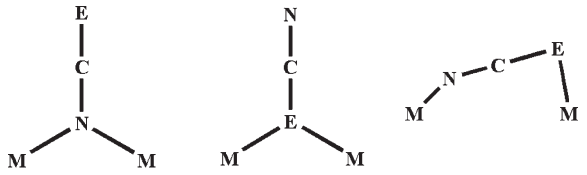

VI $\mu_{1,1}$-NCE **VII** $\mu_{1,1}$-ECN **VIII** $\mu_{1,3}$-NCE

electronic delocalization between the metal-based centers. From the values of $\Delta E_{1/2}$ (in millivolts), comproportionation constants (K_C) that provide a measurement of the stability of the mixed-valence species can be obtained using the relationship $K_C = e^{\Delta E_{1/2}/25.69}$.[5,10,11]

Recently, it was found that under certain conditions electronic communication between dimetal units may be greatly enhanced by using linkers with sulfur- instead of oxygen-containing donor atoms because of available pathways using $d\pi-d\delta$ interactions from the electrons in the δ orbitals of the Mo_2 units to the sulfur atoms.[12] In this work, the effect of pseudohalide ligands NCE^-, E = O, S, and Se, on the electronic communication between dimolybdenum units was investigated. It should be noted that, since pseudohalide groups can coordinate to transition metal atoms in different ways, for example, as a terminal, or as a bridging ligand in end-on (**VI** and **VII**) or end-to-end (**VIII**) fashions between metal atoms (Scheme 3), they offer additional possibilities to tune and control electronic communication. The *dimers of dimers* having $[Mo_2]$ with the pseudohalides NCO^-, NCS^-, and $NCSe^-$ indeed show a variety of structures. The compounds synthesized and crystallographically characterized include a simple dinuclear species containing a quadruple bond, $(Bu^n_4N)_2[Mo_2(cis\text{-}DAniF)_2(NCS)_4]$ (**1**), and the cuboidal complexes $[Mo_2(cis\text{-}DAniF)_2]_2(\mu_{1,1}\text{-}NCO)_4$ (**2**), $[Mo_2(cis\text{-}DAniF)_2]_2(\mu_{1,3}\text{-}NCS)_4$ (**3**), and $[Mo_2(cis\text{-}DAniF)_2]_2(\mu_{1,3}\text{-}NCSe)_4$ (**4**). The oxidized species $\{[Mo_2(cis\text{-}DAniF)_2]_2(\mu_{1,1}\text{-}NCO)_4\}PF_6$ (**2**·PF_6) was also prepared and fully characterized. Electrochemical properties for these dimolybdenum *dimers of dimers* varied greatly depending on the nature of the linker.

Results and Discussion

Syntheses. The synthesis of the *dimers of dimers* is based on the reaction of pseudohalides with the corner piece precursor $[Mo_2(cis\text{-}DAniF)_2(NCCH_3)_4]^{2+}$,[13] as shown in eq 1. This reaction is general and straightforward. The pseudohalides readily displace the labile acetonitrile molecules from the dimetal unit and bring the two $[Mo_2]$ units together. This procedure resembles that for the cuboidal clusters of the type $[Mo_2(cis\text{-}DAniF)_2]_2(\mu\text{-}X)_4$ (**V**), X = Cl, Br, and I,[9] which were prepared in either acetonitrile or ethanol solutions.

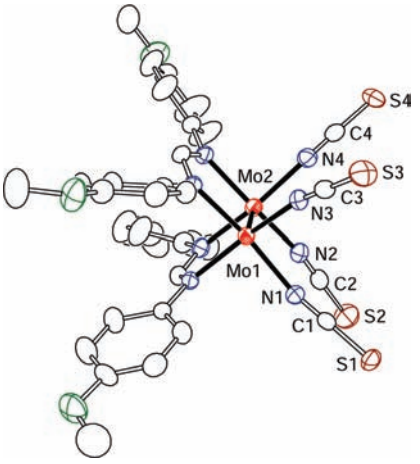

Figure 1. Core structure of the anion in **1**. All hydrogen atoms have been omitted for clarity.

$$2[Mo_2(cis\text{-}DAniF)_2(NCCH_3)_4](BF_4)_2 + 4(Bu^n_4N)X \rightarrow [Mo_2(cis\text{-}DAniF)_2]_2(\mu\text{-}X)_4 + 4(Bu^n_4N)BF_4, X = \text{halide or pseudohalide} \quad (1)$$

The cuboidal compounds **2** and **4** were prepared from the reactions in ethanol of the building block with the salts $Bu^n_4N(NCO)$ and K(NCSe), respectively, while the thiocyanate-containing compounds **1** and **3** were synthesized by direct assembly of the building block precursor $[Mo_2(cis\text{-}DAniF)_2(NCCH_3)_4](BF_4)_2$ using different molar ratios of the NCS^- ligand. Although generally the preparation of cuboidal compounds appears to be relatively straightforward,[9] in the latter case, the relative amount of thiocyanate is of great importance. The use of an excess of $Bu^n_4N(NCS)$ produced only **1**, while **3** was obtained as the main product when less $Bu^n_4N(NCS)$ was present in the reaction media.[14] From the reactions with the NCO^- or $NCSe^-$ ligands, dinuclear species analogous to **1** were not observed.

Because electrochemical measurements (vide infra) suggested that **2** could potentially be oxidized by ferrocenium salts to the corresponding singly oxidized species, the oxidizing reagent $(Cp_2Fe)PF_6$ was used at low temperatures, producing the singly oxidized species $\{[Mo_2(cis\text{-}DAniF)_2]_2(\mu_{1,1}\text{-}NCO)_4\}PF_6$ (**2**·PF_6).

Finally, it should be noted that the dimolybdenum species **1** is very air-sensitive,[15] while the cuboidal species (**2**, **3**, and **4**) are relatively stable in the air. Upon exposure to the air, the reddish purple solutions of **1** changed immediately to a red and then to a brownish red solution containing as yet unidentified species.

Structural Results. Compound **1** crystallizes in triclinic space group $P\bar{1}$ with $Z = 2$. Each of the two $(Bu^n_4N)^+$

(12) See, for example: (a) Chisholm, M. H.; Patmore, N. J. *Dalton Trans.* **2006**, 3164. (b) Cotton, F. A.; Li, Z.; Liu, C. Y.; Murillo, C. A. *Inorg. Chem.* **2007**, *46*, 7840. (c) Cotton, F. A.; Li, Z.; Liu, C. Y.; Murillo, C. A. *Inorg. Chem.* **2007**, *46*, 9294.

(13) Chisholm, M. H.; Cotton, F. A.; Daniels, L. M.; Folting, K.; Huffman, J. C.; Iyer, S. S.; Lin, C.; Macintosh, A. M.; Murillo, C. A. *J. Chem. Soc., Dalton Trans.* **1999**, 1387.

(14) Compound **3** was purified by washing the mixture with ethanol followed by crystallization. This process must be done diligently to avoid the formation of crystals of **3** that were contaminated with the starting material $[Mo_2(cis\text{-}DAniF)_2(NCCH_3)_4](BF_4)_2$.

(15) Because of the high air sensitivity of **1**, ^1H NMR spectra were obtained by adding a very small amount of cobaltocene to the respective solutions.

Table 1. Selected Bond Distances (Å) and Angles (deg) for **1**

Mo(1)−Mo(2)	2.1251(6)	C(2)−S(2)	1.625(4)
Mo(1)−N(1)	2.123(3)	C(3)−S(3)	1.634(4)
Mo(2)−N(2)	2.141(3)	C(4)−S(4)	1.630(4)
Mo(1)−N(3)	2.138(3)	Mo(1)−N(1)−C(1)	172.3(3)
Mo(2)−N(4)	2.135(3)	Mo(2)−N(2)−C(2)	167.1(3)
Mo−N_{DAniF} (av)	2.122[3]	Mo(3)−N(3)−C(3)	163.9(3)
N(1)−C(1)	1.155(4)	Mo(4)−N(4)−C(4)	161.3(3)
N(2)−C(2)	1.155(4)	N(1)−C(1)−S(1)	179.8(4)
N(3)−C(3)	1.157(4)	N(2)−C(2)−S(2)	179.1(3)
N(4)−C(4)	1.159(4)	N(3)−C(3)−S(3)	179.2(3)
C(1)−S(1)	1.615(4)	N(4)−C(4)−S(4)	179.6(4)

cations and the anion reside on a general position. The anion, shown in Figure 1, is composed of a quadruply bonded dimolybdenum unit supported by two cisoid formamidinate groups that occupy four equatorial positions, with the remaining equatorial positions occupied by four NCS^- ligands; the axial positions are unoccupied. The Mo−Mo distance of 2.1251(6) Å (Table 1) is longer than those in paddlewheel compounds containing Mo_2^{4+} units, for example, $Mo_2(O_2CCH_3)_4$ and $Mo_2(DAniF)_4$, for which the Mo−Mo distances are usually in the range of 2.08−2.10 Å,[16] but slightly shorter than those in analogous compounds with two cisoid bridging groups and four equatorial monodentate ligands such as $[Mo_2(cis\text{-}DAniF)_2(CH_3CN_{eq})_4(CH_3CN_{ax})_2]^{2+}$ (2.1439(6) Å) and $[Mo_2(cis\text{-}O_2CCH_3)_2(CH_3CN_{eq})_4(CH_3CN_{ax})_2]^{2+}$ (2.134(2) Å).[17] For the latter cationic species, the slightly longer Mo−Mo bond distances are probably due to the presence of axial ligands located at a distance of ca. 2.6 Å from the Mo atoms.

Compound **2** crystallizes in the monoclinic space group $P2_1/c$ with $Z = 2$, with the molecule being on a crystallographic inversion center. The core of the structure, shown in Figure 2, consists of two $[Mo_2]$ units linked by four NCO groups in an end-on bridging fashion, with the N atoms from the cyanate groups serving as the bridging groups, as shown by an analysis of the displacement parameters from X-ray crystallography.[18] The average N−C bond distance of 1.173[6] Å as well as the average C−O distances of 1.186[6] Å are also consistent with the bridging atom being nitrogen. Further evidence supporting the bridging nature of the N atoms was provided by IR data. A very intense peak at 2189 cm^{-1} has been assigned to the antisymmetric stretching (ν_{CN}). The pseudosymmetric stretching (ν_{CO}) was observed at 1300 cm^{-1}, and the bending mode (δ_{NCO}) at 621 cm^{-1}. For comparison, the three normal IR vibration modes for the free cyanate anion occur at 2160 (s), (1296, 1204) (m), and (635, 628) (m) cm^{-1}, respectively.[19] For **2**, the positive shifts of ν_{CN} and ν_{CO} bands and the presence of a single ν_{CO} band are consistent with the model in which the N atoms in the isocyanate ligands are coordinated to metal ions.

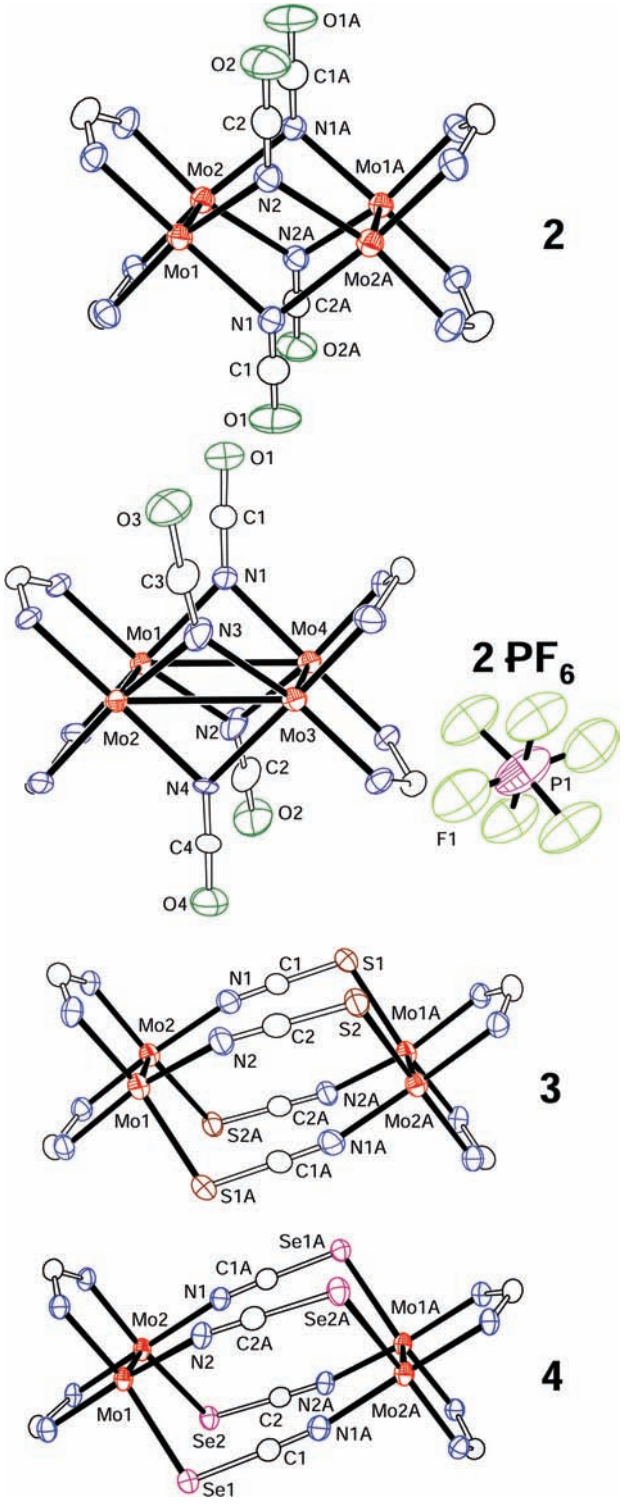

Figure 2. Core structures of **2**, **2**·PF_6, **3**·$3CH_2Cl_2$, and **4**·CH_2Cl_2 drawn with ellipsoids at the 40% probability level. All hydrogen atoms, solvent molecules, and *p*-anisyl groups have been omitted for clarity.

(16) Cotton, F. A.; Daniels, L. M.; Hillard, E. A.; Murillo, C. A. *Inorg. Chem.* **2002**, *41*, 2466.

(17) (a) Cotton, F. A.; Reid, A. H.; Schwotzer, W. *Inorg. Chem.* **1985**, *24*, 3965. (b) Pimblett, G.; Garner, C. D. *J. Chem. Soc., Dalton Trans.* **1986**, 1257.

(18) To determine whether the cyanate groups were O- or N-bonded, refinements using both models were done and compared. When the model used had O atoms as bridges, the R1 and wR2 values for all data were 0.0363 and 0.0787, respectively. The average isotropic atomic displacement parameters for both terminal N atoms and bridging O atoms in the NCO groups were about the same (0.05). For the model using N atoms as bridges, the R1 and wR2 values for the same data were about 9% and 14% lower (0.0332 and 0.0688, respectively.) Average isotropic atomic displacement parameters were 0.03 for bridging N and 0.07 for O atoms of the NCO groups. Because terminal nonbridging atoms are expected to possess a higher degree of libration than the atoms bridging the dimolybdenum units, the latter values are far more reasonable. These crystallographic data clearly support the N atoms, rather than the O atoms, being the bridging atoms.

(19) Bailey, R. A.; Kozak, S. L. *J. Inorg. Nucl. Chem.* **1969**, *31*, 689.

Table 2. Selected Bond Distances (Å) and Angles (deg) for the Pseudohalide NCE (E = O, S, Se) Bridged Cuboidal Species **2**, **2**·PF_6, **3**·$3CH_2Cl_2$, and **4**·CH_2Cl_2

	2 (E = O)	**2**·PF_6 (E = O)	**3**·$3CH_2Cl_2$ (E = S)	**4**·CH_2Cl_2 (E = Se)
Mo(1)−Mo(2)	2.1149(5)	2.137(2)	2.1268(9)	2.1246(6)
$Mo_2\cdots Mo_2$[a]	3.346	3.138	5.722	5.866
Mo(1)−N(1)	2.215(2)	2.23(1)		
Mo(1)−N(2)	2.238(2)	2.15(1)	2.153(7)	2.152(5)
Mo(2)−N(1)			2.144(7)	2.162(5)
Mo(2A)−N(1)	2.231(2)			
Mo(2A)−N(2)	2.234(2)			
Mo−N_{DAniF} (av)	2.102(2)	2.07(2)	2.108(7)	2.103(5)
N(1)−C(1)	1.161(4)	1.18(2)	1.161(10)	1.147(7)
N(2)−C(2)	1.185(4)	1.22(2)	1.151(10)	1.152(7)
C(1)−E(1)	1.195(4)	1.15(2)	1.650(8)	1.819(6)
C(2)−E(2)	1.178(4)	1.17(2)	1.648(8)	1.815(6)
Mo(1)−E(1)			2.590(2)	2.6877(7)
Mo(2)−E(2)			2.550(2)	2.6750(8)
Mo(1)−N(1)−C(1)			162.8(6)	165.8(4)
Mo(1)−N(2)−C(2)			165.7(6)	169.7(4)
N(1)−C(1)−E(1)	178.8(3)	178(2)	179.4(7)	178.0(5)
N(2)−C(2)−E(2)	177.9(3)	172(2)	178.3(7)	177.8(5)
Mo(1)−N(1)−Mo(2A)	97.64(9)			
Mo(2)−N(2)−Mo(1A)	96.87(9)			
Mo(1)−N(1)−Mo(4)		89.6(5)		
Mo(2)−N(2)−Mo(4)		94.2(5)		
C(1)−E(1)−Mo(1)			102.3(3)	99.9(2)
C(2)−E(2)−Mo(2)			102.0(3)	98.2(2)

[a] Distance between the midpoints of the two dimetal units.

Table 3. Electrochemical Data for Cuboidal $[Mo_2(DAniF)_2]_2(\mu\text{-L})_4$ Compounds[a]

L	$Mo_2\cdots Mo_2$ (Å)	$E_{1/2}(+1/0)^b$ (mV)	$E_{1/2}(+2/+1)^b$ (mV)	$\Delta E_{1/2}$ (mV)	K_C[c]	ref
OMe	3.245	−338	216	554	2.3×10^9	20
OEt	3.241	−418	169	587	8.4×10^9	20
Cl	3.601	260	800	540	1.3×10^9	9
Br	3.697	314	813	499	2.7×10^8	9
I	3.915	350	790	440	2.7×10^7	9
$\mu_{1,1}$-NCO (**2**)	3.346	226	717	491	2.0×10^8	this work
$\mu_{1,3}$-NCS (**3**)	5.722	610	970	360	1.2×10^6	this work
$\mu_{1,3}$-NCSe (**4**)	5.866	653	961	308	1.6×10^5	this work

[a] All potentials are referenced to Ag/AgCl. [b] $E_{1/2} = (E_{pa} + E_{pc})/2$ obtained from the CV. [c] K_C was estimated using the formula $K_C = \exp(\Delta E_{1/2}/25.69)$. See ref 23b.

The idealized D_{2h} symmetry for the core of **2** resembles those in the cuboidal halide and alkoxide-bridged clusters $[Mo_2(cis\text{-DAniF})_2]_2(\mu\text{-X})_4$ (X = OMe, OEt, Cl, Br, and I).[9,20] The crystallographically equivalent Mo−Mo quadruple bond distances, 2.1149(5) Å (Table 2), are similar to those in the halide-bridged tetranuclear species (2.117−2.119 Å).[9] The nonbonding separation between the midpoints of the quadruple bonds in **2** of 3.346 Å is significantly shorter than those in halide-bridged *dimers of dimers* (3.6∼3.9 Å)[9] but slightly longer than those in the alkoxide-bridged analogues (ca. 3.24 Å)[20], which is consistent with the difference in atomic radii of the bridging atoms (Table 3).

Removal of one electron from **2** gives the complex cation in **2**·PF_6, shown in Figure 2. Upon oxidation, the Mo−Mo bond distances are lengthened from 2.1149(5) Å in the precursor to 2.137(2) Å (Table 2), which is in agreement with the electron being removed from a bonding orbital delocalized over the dimetal units and a formal decrease of 0.25 in each bond order. The increase of 0.022 Å in the Mo−Mo bond distance in going from **2** to **2**·PF_6 is similar to those observed in other delocalized species[21] but considerably less than those found in localized mixed-valence complexes $[Mo_2]^+$-L$[Mo_2]^0$.[8j] Accompanying the lengthening of the metal−metal bond, the $Mo_2\cdots Mo_2$ distance is reduced by 0.21 Å, and the average bridging angles Mo−$N_{cyanate}$−Mo (ca. 91.9°) become slightly smaller than those in **2** (ca. 97.3°). This behavior is analogous to that observed in cuboidal $[Mo_2(cis\text{-DAniF})_2]_2(\mu\text{-X}_4)$ (X = Cl, Br, and I) compounds when an electron is removed from the neutral complex.[9]

The thiocyanate compound **3**, shown in Figure 2, has a tetranuclear species linked by four NCS^- ligands in an end-to-end fashion, a structure that differs significantly from that in the cyanate species. The Mo−Mo distances of 2.1268(9) Å resemble that in **2** (Table 2), but the nonbonding $Mo_2\cdots Mo_2$ separation between the midpoints of the quadruply bonded units of 5.722 Å is more than 2 Å longer than that in **2**. The selenocyanate compound **4** (Figure 2) has a similar core structure to that in **3** where the $NCSe^-$ ligands bridge two crystallo-

(20) Cotton, F. A.; Li, Z.; Liu, C. Y.; Murillo, C. A.; Zhao, Q. *Inorg. Chem.* **2006**, *45*, 6387.

(21) Cotton, F. A.; Li, Z.; Liu, C. Y.; Murillo, C. A.; Villagrán, D. *Inorg. Chem.* **2006**, *45*, 767.

graphically equivalent Mo_2 units in an end-to-end fashion. The two Mo−Mo distances of 2.1246(6) Å are essentially the same as those in **2** and **3**. The nonbonding $Mo_2\cdots Mo_2$ separation between the midpoints of the quadruply bonded units, 5.866 Å, is the longest distance thus far observed among analogous compounds having two linked Mo_2^{4+} units bridged by four anions. As shown in Table 3, in the halide and alkoxide analogues, the two Mo_2^{4+} units are separated by only 3.24−3.92 Å. This long separation between dimolybdenum units is not conducive to a good electronic communication (vide infra).

Several attempts to isolate the singly oxidized species of **3** and **4** failed because their instability prevented separation of the mixed valence species and their corresponding parent compounds. However, evidence for their existence was obtained from electron paramagnetic resonance (EPR) and near-infrared (NIR) studies (vide infra).

Electrochemistry and Electronic Communication. Electrochemical data have been commonly and conveniently used to categorize the mixed-valence compounds using the Robin and Day classification[22] and provide useful information about the degree of the interaction between redox centers.[23] However, these data have mainly been utilized in the study of systems in which the two metal-containing units are joined by only one linker. To a first approximation, it is expected that the general trends would be valid for analogous systems having more than one linker.

For the cuboidal compounds **2**, **3**, and **4**, the cyclic voltammograms (CVs) and differential pulse voltammograms (DPVs) all show two well-separated reversible waves, and the two redox processes are [Mo_2]-centered (vide infra). These processes correspond to the oxidation of each neutral compound to a singly oxidized $\{[Mo_2](\mu\text{-pseudohalide})_4[Mo_2]\}^+$ and a doubly oxidized $\{[Mo_2](\mu\text{-pseudohalide})_4[Mo_2]\}^{2+}$ species. Electrochemical measurements for **2** (Figure 3) show two successive one-electron oxidations separated by a relatively large $\Delta E_{1/2}$ value of 491 mV. Previous studies on these systems have shown that the direct σ interaction between the frontier δ orbitals of the two dimetal centers plays an important role in the coupling effect when the nonbonding $Mo_2\cdots Mo_2$ separations are less than 5.7 Å.[9b,20] The $\Delta E_{1/2}$ value of 491 mV for **2**, which has an $Mo_2\cdots Mo_2$ separation of 3.346, follows the general trend of other cuboidal complexes of the type $[Mo_2(cis\text{-DAniF})_2]_2(\mu\text{-X})_4$ (X = OEt and OMe) listed in Table 3. It should be noted that previous studies[9b] had shown that the direct δ-to-δ orbital interaction becomes negligible when the $Mo_2\cdots Mo_2$ separation exceeds 5.7 Å. Therefore, very small $\Delta E_{1/2}$ values for **3** and **4** are anticipated; the observed $\Delta E_{1/2}$ values 360 and 308 mV are mainly due to a weak electrostatic repulsion.

For the dinuclear compound **1**, the CV and DPV are shown in Figure 4. The two processes correspond to the successive oxidation to $\mathbf{1}^+$ and $\mathbf{1}^{2+}$. The first oxidation process (−85 mV) is not unusual for species containing quadruple-bonded dimolybdenum units spanned by formamidinate units,[24] but the second one (812 mV) is very

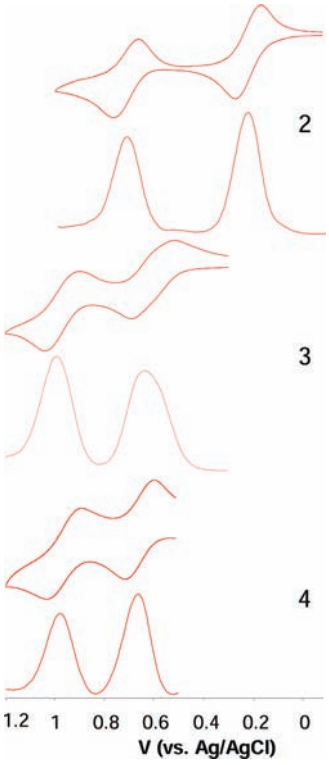

Figure 3. CVs and DPVs for **2**, $\mathbf{3}\cdot 3CH_2Cl_2$, and $\mathbf{4}\cdot CH_2Cl_2$ in CH_2Cl_2 solution. The potentials, in volts, are referenced to Ag/AgCl.

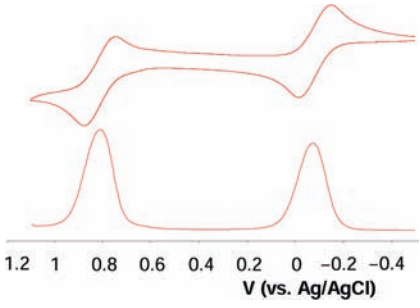

Figure 4. CV and DPV for **1** in CH_2Cl_2 solution. The potentials, in volts, are referenced to Ag/AgCl.

unusual as only a handful of species containing Mo_2^{6+} units derived from tetragonal paddlewheel cores are known.[25] Examples include $Mo_2(guanidinate)_4^{2+}$,[26] $Mo_2(HPO_4)_4^{2-}$,[27] and $Mo_2[Mo_2(CO)_4(PhPO_2)_2]_2^{2-}$ species.[28]

EPR and NIR Spectra. The X-band EPR spectra for $\mathbf{1}^+$ (Figure 5) prepared in situ by the reaction of **1** with

(22) Robin, M. B.; Day, P. *Adv. Inorg. Chem. Radiochem.* **1967**, *10*, 357.
(23) (a) Cannon, R. D. *Electron-Transfer Reactions*; Butterworth: London, 1980. (b) Richardson, D. E.; Taube, H. *Inorg. Chem.* **1981**, *20*, 1278.
(24) Lin, C.; Protasiewicz, J. D.; Ren, T. *Inorg. Chem.* **1996**, *35*, 6422.
(25) Cotton, F. A.; Murillo, C. A.; Walton, R. A. *Multiple Bonds Between Metal Atoms*; Springer Science and Business Media, Inc.: New York, 2005.
(26) (a) Bailey, P. J.; Bone, S. F.; Mitchell, L. A.; Parsons, S.; Taylor, K. J.; Yellowlees, L. J. *Inorg. Chem.* **1997**, *36*, 867. (b) Cotton, F. A.; Daniels, L. M.; Murillo, C. A.; Timmons, D. J.; Wilkinson, C. C. *J. Am. Chem. Soc.* **2002**, *124*, 9249. (c) Cotton, F. A.; Murillo, C. A.; Wang, X.; Wilkinson, C. C. *Dalton Trans.* **2006**, 4623. (d) Cotton, F. A.; Durivage, J. C.; Gruhn, N. E.; Lichtenberger, D. L.; Murillo, C. A.; Van Dorn, L. O.; Wilkinson, C. C. *J. Chem. Phys. B* **2006**, *110*, 19793.
(27) (a) Bino, A.; Cotton, F. A. *Angew. Chem., Int. Ed. Engl.* **1979**, *18*, 462. (b) Bino, A.; Cotton, F. A. *Inorg. Chem.* **1979**, *18*, 3562. (c) Chang, I.-J.; Nocera, D, G. *J. Am. Chem. Soc.* **1987**, *109*, 4901.
(28) Cotton, F. A.; Daniels, L. M.; Liu, C. Y.; Murillo, C. A.; Schultz, A. J; Wang, X. *Inorg. Chem.* **2002**, *41*, 4232.

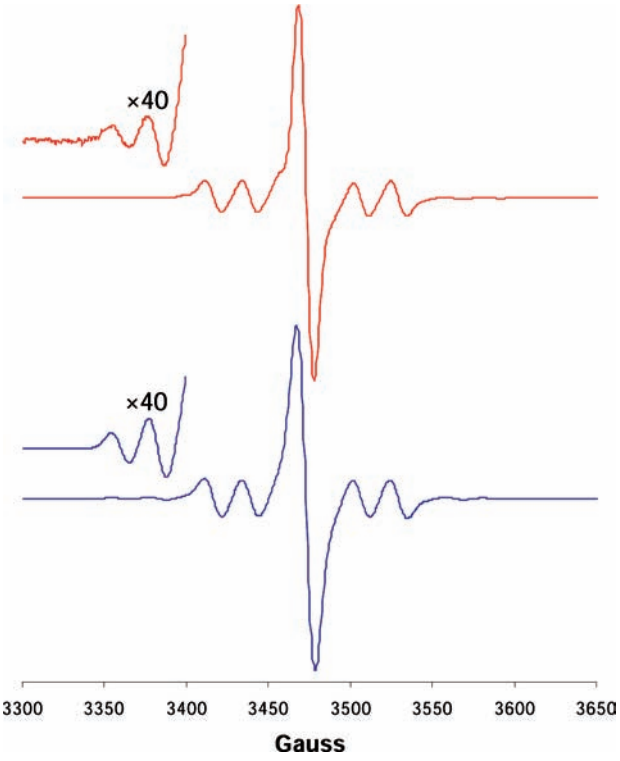

Figure 5. X-band EPR spectrum of $\mathbf{1}^+$ produced by in situ reaction of the precursor **1** and $(Cp_2Fe)BF_4$ in CH_2Cl_2 at ambient temperature (red trace). ν = 9.46 GHz, g_{iso} = 1.946, A_{iso} = 20.5 × 10^{-4} cm^{-1}. The blue trace below is the simulated spectrum.

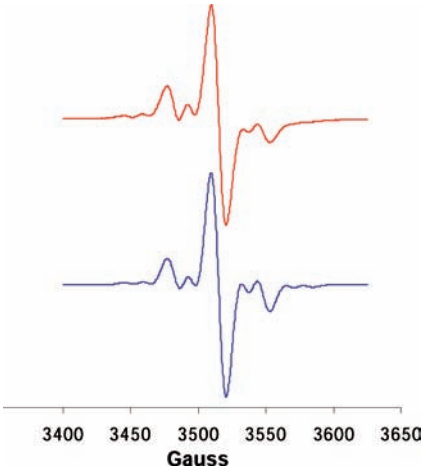

Figure 6. X-band EPR spectrum of $\mathbf{2}\cdot PF_6$ in CH_2Cl_2 at ambient temperature (red). ν = 9.47 GHz, g_{iso} = 1.925, A_{iso} = 11.6 × 10^{-4} cm^{-1}. The blue trace below is the simulated spectrum.

1 equiv of $(Cp_2Fe)BF_4$, $\mathbf{2}\cdot PF_6$ (Figure 6), and $\mathbf{3}^+$ (Figure 7) prepared by in situ oxidation of **3** with 1 equiv of $(NO)BF_4$ were measured at room temperature in a CH_2Cl_2 solution. Only one prominent signal was observed for each complex, which is consistent with a doublet electronic ground state. The *g* values of 1.946 for $\mathbf{1}^+$, 1.925 for $\mathbf{2}\cdot PF_6$, and 1.947 for $\mathbf{3}^+$ are significantly different from that for an organic free radical and indicate that the unpaired electron resides in a mainly metal-based orbital. The main signal is due to the molecules containing only the ^{96}Mo (I = 0) isotope (about 74% abundance), whereas the small peaks flanking the main

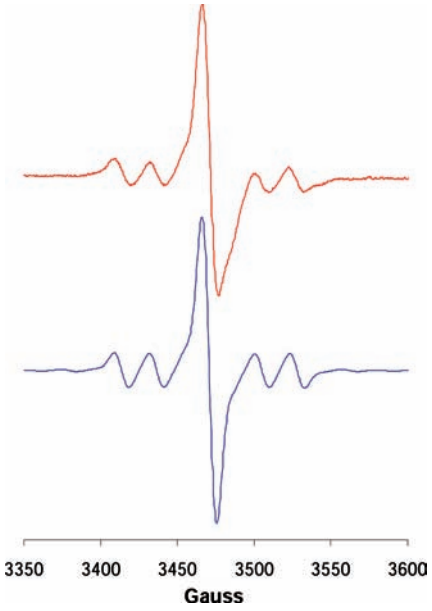

Figure 7. X-band EPR spectrum of $\mathbf{3}^+$ produced by in situ reaction of the precursor **3** and $(NO)BF_4$ in CH_2Cl_2 at ambient temperature (red). ν = 9.47 GHz, g_{iso} = 1.947, A_{iso} = 20.8 × 10^{-4} cm^{-1}. The blue trace below is the simulated spectrum.

signal are due to coupling of four Mo $^{95,97}Mo$ (I = 5/2) isotopes that have a combined natural abundance of about 25%.

For $\mathbf{1}^+$, a spectral simulation was done using a model with one odd electron residing on a Mo_2 unit. As shown in Figure 5, the parameters g = 1.946 and A = 20.5 × 10^{-4} cm^{-1} were used, similar to those in the parent paddlewheel cation $[Mo_2(DAniF)_4]^+$.[29] These results show satisfactory agreement with the results obtained from electrochemistry, in which the first reversible oxidation (−85 mV) corresponds to the $\mathbf{1}^{(0/1+)}$ process, while the second oxidation (812 mV) corresponds to the $\mathbf{1}^{(1+/2+)}$ process.

The EPR spectrum for the singly oxidized species $\mathbf{2}\cdot PF_6$ exhibits a prominent peak (g = 1.925) and several hyperfine lines (Figure 6). Simulation gives a hyperfine coupling constant A of 11.6 × 10^{-4} cm^{-1}, which is about half of that for $\mathbf{1}^+$. Prior studies on various mixed-valence species of the type $\{[Mo_2]L[Mo_2]\}^+$ have shown that electronic delocalization over two Mo_2 units has the effect of lowering the constant A. For example, for the delocalized complexes $\{[Mo_2]$-(dioxolenate)$[Mo_2]\}^+$,[30] the hyperfine coupling constant A was 12.2 × 10^{-4} cm^{-1} . Similarly, $\{\beta$-$[Mo_2]$(oxamidate)-$[Mo_2]\}^+$ has a hyperfine coupling constant A of 11 × 10^{-4} cm^{-1},[31] while for the weakly coupled compound, $\{[Mo_2](N,N'$-diethylterephthalamidate)$[Mo_2]\}^+$[32] and $\{\alpha$-$[Mo_2]$(oxamidate)$[Mo_2]\}^+$,[31] the A values are 22 × 10^{-4} cm^{-1} and 21 × 10^{-4} cm^{-1}, respectively. These data are again consistent with the electron being delocalized over the two $[Mo_2]$ units in $\mathbf{2}\cdot PF_6$.

(29) Cotton, F. A.; Donahue, J. P.; Huang, P.; Murillo, C. A.; Villagrán, D.; Wang, X. *Z. Anorg. Allg. Chem.* **2005**, *631*, 2606.
(30) Cotton, F. A.; Murillo, C. A.; Villagrán, D.; Yu, R. *J. Am. Chem. Soc.* **2006**, *128*, 3281.
(31) Cotton, F. A.; Liu, C. Y.; Murillo, C. A.; Zhao, Q. *Inorg. Chem.* **2007**, *46*, 2604.
(32) Cotton, F. A.; Li, Z.; Liu, C. Y.; Murillo, C. A. *Inorg. Chem.* **2006**, *45*, 9765.

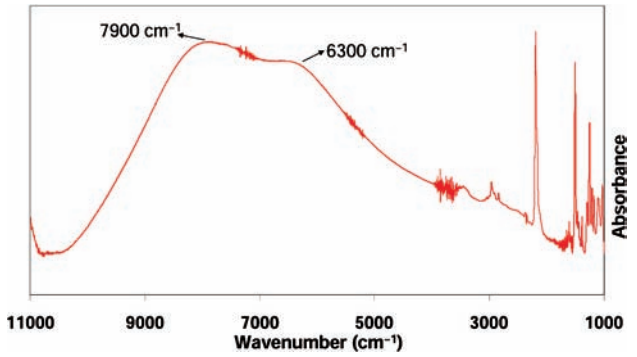

Figure 8. Near-IR spectrum of the crystalline mixed-valence species $\mathbf{2}\cdot PF_6$ in KBr pellets.

The spectrum of the singly oxidized species $\mathbf{3}^+$ also exhibits a prominent peak and several hyperfine lines (Figure 7). Simulations give a hyperfine coupling constant A of 20.8×10^{-4} cm^{-1}, which is similar to that for $\mathbf{1}^+$ and those in localized $\{[Mo_2]^+L[Mo_2]\}$ species mentioned above. This indicates that the electron is localized in only one of the $[Mo_2]$ units on the time scale of the EPR measurements at 9.5 GHz (1.68×10^{-11} s).[33]

The NIR spectrum of $\mathbf{2}\cdot PF_6$ was measured in the region from 2000 to 10 500 cm^{-1} both in the solid state using KBr pellets (Figure 8) and in CH_2Cl_2 solutions. In both media, the NIR spectra were essentially the same. The mixed valence complex shows two intense broad absorption bands centered at ca. 6300 and 7900 cm^{-1}. It is similar to the NIR spectra of the complexes $\{[Mo_2(DAniF)_2]_2(\mu\text{-}X)_4\}^+$ (X = OMe, Cl, Br, and I) where two broad absorption bands were observed in the NIR region.[9b,20] Such transitions are often referred to as intervalence charge transfer transitions. Even though the Hush formula, $\Delta\nu_{1/2} = (2310\nu_{max})^{1/2}$,[34] may not be used to interpret the spectra of these $[cis\text{-}Mo_2(DAniF)_2]_2(\mu\text{-}X)_4$ compounds, the intense bands are consistent with significant electronic interaction between the two dimolybdenum units.

No NIR bands were observed for the singly oxidized species of **3** or **4** prepared in situ by oxidizing the corresponding precursors with 1 equiv of $(NO)BF_4$. This suggests again that the odd electrons in the mixed valence systems are localized within one dimetal unit during the time scale of NIR measurements (10^{-14} s)[35] and the electronic interaction between the two dimetal units is very weak, which is also consistent with the results obtained from electrochemistry and EPR studies.

Electronic Structures and DFT Calculations. The DFT calculations were done using models with all DAniF ligands simplified as *cis*-NHCHNH and parameters from the crystal structure for complexes as starting points except **1**, which uses the crystal structure directly. The models for the cuboidal compounds were optimized by imposing C_i symmetry constraints, while the model for **1** was not constrained to any symmetry to ensure higher accuracy. Frequency calculations were performed on the optimized geometries to verify that they corresponded to minima in the potential energy surface. The general agreement between the calculated and the experimental geometric data (Tables 1, 2, 4, and 5) suggests that such simplification is reasonable. The overestimation of the Mo−Mo distances by ca. 0.05 Å is analogous to that in previous studies and is reasonable because hydrogen atoms instead of the basic *p*-anisyl groups were used for the calculations.[36]

Analysis of the frontier orbitals of **1** (Figure 9) shows that the HOMO is a metal-based δ orbital (53.48%).[37] There is also a large percentage of thiocyanate ligand contribution (29.15%). The antibonding π^* character between the δ orbital of $[Mo_2]$ unit and p orbitals from the cyanate ligands pushes the HOMO up in energy. This

Table 4. Calculated Bond Distances (Å) and Angles (deg) for **1** from DFT Calculations

Mo(1)−Mo(2)	2.174	C(2)−S(2)	1.640
Mo(1)−N(1)	2.121	C(3)−S(3)	1.640
Mo(2)−N(2)	2.120	C(4)−S(4)	1.642
Mo(1)−N(3)	2.122	Mo(1)−N(1)−C(1)	170.43
Mo(2)−N(4)	2.120	Mo(2)−N(2)−C(2)	170.74
$Mo-N_{DAniF}$ (av)	2.151	Mo(3)−N(3)−C(3)	170.12
N(1)−C(1)	1.200	Mo(4)−N(4)−C(4)	169.86
N(2)−C(2)	1.200	N(1)−C(1)−S(1)	178.10
N(3)−C(3)	1.200	N(2)−C(2)−S(2)	178.16
N(4)−C(4)	1.200	N(3)−C(3)−S(3)	177.75
C(1)−S(1)	1.640	N(4)−C(4)−S(4)	178.96

Table 5. Calculated Bond Distances (Å) and Angles (deg) for the Models of **2**, $\mathbf{2}\cdot PF_6$, **3**, and **4** with *Ci* Symmetry Using DFT Calculations

		$\mathbf{2}\cdot PF_6$		
	2 (E = O)	(E = O)	**3** (E = S)	**4** (E = Se)
Mo(1)−Mo(2)	2.162	2.182	2.169	2.170
$Mo_2\cdots Mo_2$[a]	3.369	3.225	5.777	5.900
Mo(1)−N(1)	2.250	2.210		
Mo(1)−N(2)	2.247	2.210		
Mo(1)−N(2)			2.145	2.147
Mo(2)−N(1)			2.146	2.147
Mo(2A)−N(1)	2.248	2.210		
Mo(2A)−N(2)	2.249	2.210		
$Mo-N_{DAniF}$ (av)	2.086	2.088	2.093	2.095
N(1)−C(1)	1.226	1.231	1.190	1.188
N(2)−C(2)	1.226	1.231	1.190	1.188
C(1)−E(1)	1.211	1.202	1.663	1.813
C(2)−E(2)	1.211	1.202	1.663	1.813
Mo(1)−E(1)			2.664	2.763
Mo(2)−E(2)			2.662	2.764
Mo(1)−N(1)−C(1)			166.83	169.44
Mo(1)−N(2)−C(2)			166.58	169.15
N(1)−C(1)−E(1)	178.63	178.94	176.87	175.58
N(2)−C(2)−E(2)	178.64	178.95	176.69	175.83
Mo(1)−N(1)−Mo(2A)	97.05	93.71		
Mo(2)−N(2)−Mo(1A)	97.08	93.71		
C(1)−E(1)−Mo(1)			101.32	99.13
C(2)−E(2)−Mo(2)			101.52	99.10

[a] Distance between the midpoints of the two dimetal units.

(33) The time scale is given by $(2\pi\nu)^{-1}$, where ν is the operating frequency. See: (a) Weil, J. A.; Bolton, J. R.; Wertz, J. E. *Electron Paramagnetic Resonance Spectroscopy: Elementary Theory and Practical Applications*; Wiley: New York, 1994. (b) Dei, A.; Gatteschi, D.; Sangregorio, C.; Sorace, L.; Vaz, M. G. F. *Chem. Phys. Lett.* **2003**, *368*, 162.

(34) The Hush formula is only appropriate for systems with two dimetal units linked by *one* linker. See: Hush, N. S. *Coord. Chem. Rev.* **1985**, *64*, 135.

(35) Lever, A. B. P. In *Comprehensive Coordination Chemistry II*; McCleverty, J. A., Meyer, T. J., Eds.; Elsevier Science: Oxford, U. K., 2004; Vol. *2*, pp. 435−438.

(36) Cotton, F. A.; Donahue, J. P.; Murillo, C. A.; Pérez, L. M. *J. Am. Chem. Soc.* **2003**, *125*, 5486.

(37) Percentage of orbital characters are calculated from the equation $a^2/(a^2 + b^2 + c^2 + ...)$ where a, b, c... are the coefficients from the DFT calculations for each atomic orbital.

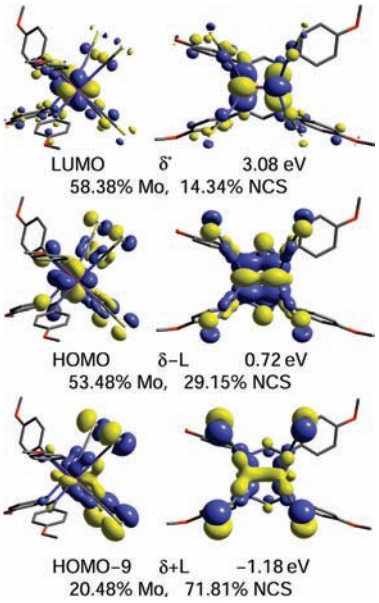

Figure 9. Selected frontier orbitals for the model of the anion in **1**, $[Mo_2(cis\text{-}DAniF)_2(NCS)_4]^{2-}$. Front view (left) and side view (right) are shown using isosurface values of 0.03.

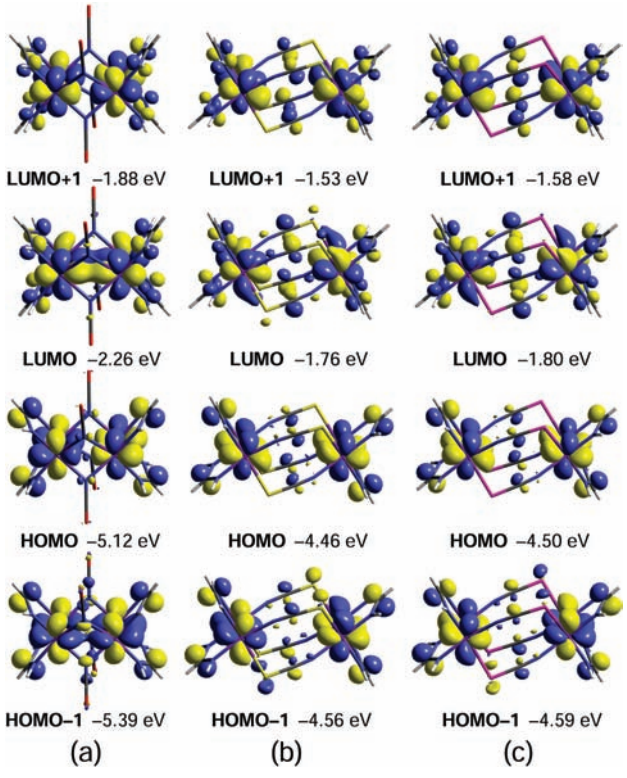

Figure 10. Selected frontier orbitals for the models $[Mo_2(cis\text{-}NHCHNH)_2]_2(\mu_{1,1}\text{-}NCO)_4$ (a), $[Mo_2(cis\text{-}NHCHNH)_2]_2(\mu_{1,3}\text{-}NCS)_4$ (b), and $[Mo_2(cis\text{-}NHCHNH)_2]_2(\mu_{1,3}\text{-}NCSe)_4$ (c) using isosurface values of 0.03.

allows electrochemical observation of the two oxidation processes to $\mathbf{1}^+$ and $\mathbf{1}^{2+}$.

For the model of **2**, the frontier orbitals from the DFT calculations (Figure 10) are analogous to those in other cuboidal tetranuclear clusters $[Mo_2(cis\text{-}DAniF)_2]_2(\mu\text{-}X)_4$ (X = OEt, OMe, Cl, Br, and I).[9b,20] The direct σ interaction through space between the δ orbitals in the dimetal units generates the bonding orbitals (a_g, $\delta + \delta$ and b_{2u}, $\delta^* + \delta^*$) and antibonding orbitals (b_{3u}, $\delta - \delta$ and b_{1g}, $\delta^* - \delta^*$) over the four molybdenum atoms. The orbitals from the molybdenum atoms make the largest contribution to these two sets of MOs (ca. 70∼87%). It has been established that the energy difference, ΔE, between $\delta - \delta$ and $\delta + \delta$ orbitals is a measure of the electronic interaction between the two dimetal units.[9b,20] The calculations (Table 6) show that the ΔE values are 0.28, 0.10, and 0.09 eV for **2**, **3**, and **4**, respectively. They follow the trend that the electronic coupling between the two dimetal units increases as the two dimetal units approach each other, because of the shortening of the $Mo_2\cdots Mo_2$ distances.

After one electron was removed in the cyanate-bridged complex **2**, the calculated Mo−Mo bond distances increased by about 0.02 Å, similar to the change of 0.022 Å observed in the X-ray crystallographic study. The calculated distance between the midpoints of the two $[Mo_2]$ units decreased by about 0.14 Å, which is comparable with the experimental decrease of 0.21 Å. The DFT calculations on the singly oxidized species $\mathbf{2}\cdot PF_6$ also show that the spin density of the SOMO (Figure 11) is delocalized over the two dimolybdenum units. This is consistent with the EPR spectrum of $\mathbf{2}\cdot PF_6$ that shows a low g value of 1.925. It also supports the statement that direct σ interaction between the two δ orbitals provides an efficient route for the electronic communication between the redox centers.

Conclusions

Reaction of $[Mo_2(cis\text{-}DAniF)_2(NCCH_3)_4](BF_4)_2$ with thiocyanate ligands gave either a simple dinuclear species (**1**) or a cuboidal species (**3**), depending on the molar ratio of the pseudohalide to the corner piece. The two reversible processes observed in the CV of **1** can be associated with the successive oxidation to $\mathbf{1}^+$ and a rare $\mathbf{1}^{2+}$ species. DFT calculations indicate that the thiocyanate ligands in **1** played the most important role in elevating the δ orbital energy of the dimolybdenum unit.

For the cuboidal compounds $[Mo_2(cis\text{-}DAniF)_2](NCE)_4$ with E = O, the linker binds to the dimetal units through the N atom, while for the E = S and Se isomers, the linkers span the two Mo_2^{4+} units using both E and N termini. As shown by DFT, the short separation between dimolybdenum units in the singly oxidized cyanate complex is responsible for the strong electronic communication because it allows direct σ interaction between the δ bonds in the dimolybdenum units in $\mathbf{2}^+$. For the neutral sulfur and selenium isomers, the longer separation found between the quadruple-bonded units does not allow such interactions, and the communication significantly decreases.

Experimental Section

Materials and Methods. All procedures were performed under N_2 using either a N_2 drybox or standard Schlenk techniques. Solvents were dried and then distilled under N_2 following conventional methods or under argon using a Glass Contour solvent purification system. The starting materials $[Mo_2(cis\text{-}DAniF)_2(NCCH_3)_4](BF_4)_2$[13] and HDAniF[24] were prepared following published methods. Other reagents were purchased from commercial sources and used after they were dried under a vacuum overnight.

Physical and Characterization Measurements. Elemental analyses were performed by Robertson Microlit Laboratories, Madison, New Jersey, upon crystalline samples that were dried overnight under a vacuum. ^{1}H NMR spectra were recorded at

Table 6. Comparison of ΔE Values (eV) in Cuboidal $[Mo_2(DAniF)_2]_2(\mu\text{-}L)_4$ Compounds

L	$Mo_2\cdots Mo_2$ (exp)	$Mo_2\cdots Mo_2$ (calcd)	$\Delta E_{1/2}$ (mV)	ΔE (eV)[a]	ref
$[Mo_2Cl_2(PEt_3)_2]_2(\mu\text{-}Cl)_4$	2.901(2)	2.918	N/A	3.21	50
OMe	3.245	3.333	554	0.34	20
Cl	3.601	3.706	540	0.25	9
Br	3.697	3.864	499	0.23	9
I	3.915	4.054	440	0.21	9
$\mu_{1,1}$-NCO (**2**)	3.346	3.369	491	0.28	this work
$\mu_{1,3}$-NCS (**3**)	5.722	5.777	360	0.10	this work
$\mu_{1,3}$-NCSe (**4**)	5.866	5.900	308	0.09	this work

[a] $\Delta E = E_{\delta-\delta} - E_{\delta+\delta}$.

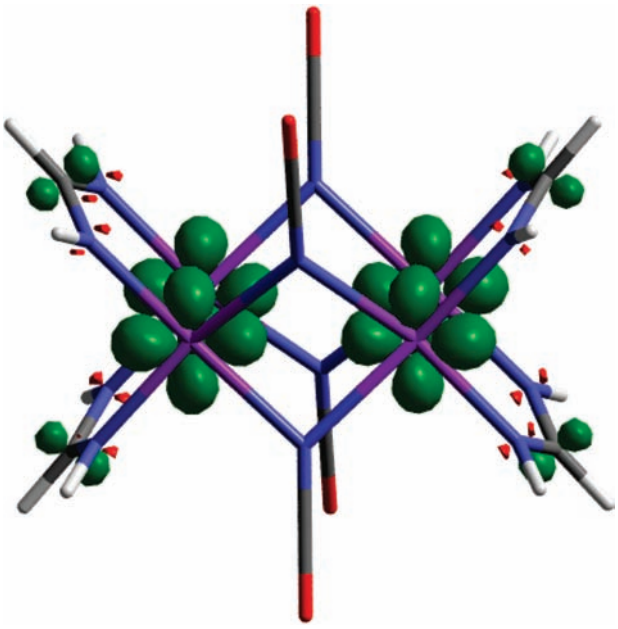

Figure 11. Spin density diagram of the SOMO in the $\mathbf{2}\cdot PF_6$ model with an isosurface value of 0.006.

25 °C on a Mercury-300 NMR spectrometer with chemical shifts (δ, ppm) referenced to the protonated solvent residue. Absorption spectra in the range of 200−800 nm were measured at ambient temperature on a Shimadzu UV-2501 PC spectrophotometer. The NIR and IR spectra were obtained on a Bruker TEASOR 27 spectrometer. EPR spectra were recorded using a Bruker ESP300 spectrometer, and spectra simulations were performed using the program WIN-EPR SimFonia provided by Bruker. The CVs and DPVs were taken using a CH Instruments Model-CH1620A electrochemical analyzer in a 0.1 M $(Bu^n_4N)PF_6$ solution in CH_2Cl_2 with Pt working and auxiliary electrodes, a Ag/AgCl reference electrode, and a scan rate of 100 mV/s (for CVs). All of the potential values are referenced to the Ag/AgCl electrode; under the present experimental conditions, the $E_{1/2}$ for the Fc^+/Fc couple consistently occurred at +440 mV in CH_2Cl_2.

Preparation of $(Bu^n_4N)_2[Mo_2(cis\text{-}DAniF)_2(NCS)_4]$, 1. To a mixture of $[Mo_2(cis\text{-}DAniF)_2(NCCH_3)_4](BF_4)_2$ (0.16 g, 0.15 mmol) and $Bu^n_4N(NCS)$ (0.25 g, 0.83 mmol) was added ethanol (15 mL). Upon stirring, a reddish purple precipitate was immediately produced. This mixture was stirred for about 4 h; the supernatant solution was then decanted. The reddish purple solid was washed with 2 × 10 mL of ethanol and then dried under a vacuum. The solid was dissolved in CH_2Cl_2, and to this solution was added a layer of hexanes. Crystals were produced in about two days. Yield: 80 mg, 74%. ^{1}H NMR (in CD_2Cl_2, ppm):[15] 8.50 (s, 2H, N−C*H*−N), 6.54 (m, 8H, aromatic), 6.51 (m, 8H, aromatic), 3.66 (s, 12H, OCH_3), 3.22 (t, 16H, N−CH_2−CH_2), 1.65 (p, 16H, CH_2−CH_2−CH_2), 1.43 (m, 16H, CH_2−CH_2−CH_3), 1.01 (t, 24H, CH_2−CH_3). UV−vis in CH_2Cl_2, λ_{max} (nm) (ε, $M^{-1}cm^{-1}$): 365 (1.0×10^3), 543 (1.1×10^4). IR (KBr, cm^{-1}): 2958 (m), 2872 (s), 2831 (s), 2343 (s), 2083 (s), 2077 (w), 1608 (s), 1543 (s), 1502 (w), 1462 (m), 1383 (s), 1305 (w), 1288 (w), 1244 (w), 1217 (w), 1176 (w), 1105 (w), 1033 (w), 930 (m), 877 (m), 825 (m), 761 (m), 644 (m), 619 (w), 590 (w), 532 (m), 507 (w). Anal. Calcd. for $C_{66}H_{102}Mo_2N_{10}O_4S_4$ (**1**): C, 55.84; H, 7.24; N, 9.87. Found: C, 55.58; H, 7.00; N, 9.71.

Preparation of $[Mo_2(cis\text{-}DAniF)_2]_2(\mu_{1,1}\text{-}NCO)_4$, 2. To a mixture of $[Mo_2(cis\text{-}DAniF)_2(NCCH_3)_4](BF_4)_2$ (0.31 g, 0.30 mmol) and $Bu^n_4N(NCO)$ (0.17 g, 0.60 mmol) was added ethanol (10 mL). Upon stirring, a greenish brown precipitate was gradually produced. This mixture was stirred overnight, and the supernatant solution was then decanted. After washing the solid with ethanol (2 × 15 mL), the greenish brown solid was collected by filtration and dried overnight under a vacuum. The solid was dissolved in CH_2Cl_2, and a layer of hexanes was then added. Many red crystals were produced after one week when the diffusion of hexanes was complete. Yield: 0.20 g, 83%. ^{1}H NMR (in $CDCl_3$, ppm): 8.80 (s, 4H, N−C*H*−N), 6.62 (m, 32H, aromatic), 3.69 (s, 24H, OCH_3). UV−vis in CH_2Cl_2, λ_{max} (nm) (ε, $M^{-1}cm^{-1}$): 493 (1.3×10^4), 591 (3.0×10^3). IR (KBr, cm^{-1}): 2964 (m), 2835 (w), 2356 (s), 2262 (s), 2189 (w), 2158 (s), 1874 (w), 1691 (m), 1609 (s), 1535 (w), 1504 (w), 1464 (m), 1439 (s), 1385 (s), 1300 (w), 1288 (w), 1250 (m), 1215 (w), 1173 (w), 1107 (w), 1036 (w), 939 (m), 825 (m), 802 (m), 766 (s), 679 (m), 621 (m), 592 (m), 530 (m), 474 (m), 451 (m). Anal. Calcd. for $C_{64}H_{60}Mo_4N_{12}O_{12}$ (**2**): C, 48.87; H, 3.84; N, 10.69. Found: C, 48.61; H, 3.68; N, 10.58.

Preparation of $\{[Mo_2(cis\text{-}DAniF)_2]_2(\mu_{1,1}\text{-}NCO)_4\}PF_6$, $\mathbf{2}\cdot PF_6$. An orange solution of **2** (0.207 g, 0.130 mmol) in 10 mL of CH_2Cl_2 and a blue solution having 1 equiv of $(Cp_2Fe)PF_6$ in 10 mL of CH_2Cl_2 were prepared separately, and each was cooled to −78 °C. The two solutions were mixed by transferring via cannula the oxidizing reagent into the solution containing the dimolybdenum complex. A dark brown solution was produced. After the resultant solution was stirred at −78 °C for 30 min, a copious amount of hexanes was added by syringe to produce a dark brown precipitate. The supernatant solution was then decanted, and the solid residue was washed with 20 mL of precooled hexanes. The solid was dissolved at room temperature in dichloromethane, and the solution was layered with hexanes. This process produced small black, block-shaped crystals. Yield: 0.16 g, 72%. UV−vis (λ_{max}, nm) (ε, $M^{-1}cm^{-1}$): 461 (3.3×10^4), 589 (3.4×10^4). NIR (KBr, cm^{-1}): 7900 (b), 6300 (b). IR (KBr, cm^{-1}): 2959 (m), 2833 (w), 2366 (w), 2345 (s), 2193 (w), 1607 (s), 1504 (s) 1458 (m), 1439 (m), 1385 (s), 1294 (w), 1250 (w), 1207 (w), 1175 (w), 1092 (w), 1030 (w), 939 (w), 829 (w), 825 (w), 800 (w), 764 (s), 588 (s), 557 (s), 519 (m). Anal. Calcd for $C_{70}H_{74}F_6Mo_4N_{12}O_{12}P$ ($\mathbf{2}\cdot PF_6\cdot$Hexane): C, 46.60; H, 4.13; N, 9.32. Found: C, 46.55; H, 3.90; N, 9.06.

Preparation of $[Mo_2(cis\text{-}DAniF)_2]_2(\mu_{1,3}\text{-}NCS)_4$, 3. This compound was synthesized similarly to **1** but using a stoichiometric deficiency of $Bu^n_4N(NCS)$ relative to that of the corner piece precursor as follows: to a mixture of $[Mo_2(cis\text{-}DAniF)_2(NCCH_3)_4](BF_4)_2$ (0.13 g, 0.12 mmol) and $Bu^n_4N(NCS)$ (0.060 g, 0.20 mmol) was added ethanol (10 mL). Upon stirring at ambient

Table 7. Crystallographic Data

compound	**1**	**2**	**2**·PF_6	**3**·$3CH_2Cl_2$	**4**·CH_2Cl_2
chemical formula	$Mo_2C_{66}H_{102}N_{10}O_4S_4$	$Mo_4C_{64}H_{60}N_{12}O_{12}$	$C_{64}H_{60}F_6Mo_4N_{12}O_{12}P$	$Mo_4C_{67}H_{66}Cl_6N_{12}O_8S_4$	$Mo_4C_{65}H_{62}Cl_2N_{12}O_8Se_4$
fw	1419.70	1573.00	1717.97	1892.02	1909.77
space group	$P\bar{1}$ (No. 2)	$P2_1/c$ (No. 14)	$P2_12_12_1$ (No. 19)	$P2_1/c$ (No. 14)	$P2_1/n$ (No. 14)
a (Å)	12.588(2)	12.914(3)	9.932(2)	13.424(2)	13.414(2)
b (Å)	14.448(3)	11.167(2)	29.776(6)	16.010(3)	15.991(2)
c (Å)	22.734(4)	22.036(5)	31.998(6)	18.649(3)	17.191(2)
α (deg)	96.263(3)	90	90	90	90
β (deg)	104.917(3)	91.272(4)	90	105.965(3)	106.449(2)
γ (deg)	109.220(3)	90	90	90	90
V (Å^3)	3686(1)	3177(1)	9462(3)	3853(1)	3536.7(7)
Z	2	2	4	2	2
d_{calcd} (g cm^{-3})	1.279	1.644	1.206	1.631	1.793
μ (mm^{-1})	0.503	0.843	0.597	1.012	2.888
T (K)	213(2)	213(2)	213(2)	213(2)	213(2)
R1[a] (wR2[b])	0.0607 (0.1113)	0.0332 (0.0688)	0.1540 (0.2674)	0.0853 (0.1854)	0.0606 (0.1185)

[a] $R1 = [\sum w(F_o - F_c)^2/\sum wF_o^2]^{1/2}$. [b] $wR2 = [\sum[w(F_o^2 - F_c^2)^2]/\sum w(F_o^2)^2]^{1/2}$, $w = 1/[\sigma^2(F_o^2) + (aP)^2 + bP]$, where $P = [\max(F_o^2,0) + 2(F_c^2)]/3$.

temperature, a red precipitate immediately formed. This mixture was stirred for about 5 h; the supernatant solution was then decanted. After washing the solid with 2 × 10 mL of ethanol, the red solid was collected by filtration and dried under a vacuum overnight. A mixture of CH_2Cl_2/hexanes was used for crystallization. Small red, block-shaped crystals were produced after about 12 h of diffusion. The red CH_2Cl_2 solution of **2** was stable in the air for about two days. Yield: 40 mg, 41%. ^{1}H NMR (in $CDCl_3$, ppm): 8.91 (s, 2H, N−C*H*−N), 8.66 (s, 2H, N−C*H*−N), 6.86 (d, 4H, aromatic), 6.74 (m, 12H, aromatic), 6.53 (m, 8 H, aromatic), 6.35 (m, 8 H, aromatic), 3.72 (s, 12H, OCH_3), 3.65 (s, 12H, OCH_3). UV−vis in CH_2Cl_2, λ_{max} (nm) (ε, M^{-1}cm^{-1}): 412 (7.0×10^3), 529 (5.1×10^3). IR (KBr, cm^{-1}): 2951 (m), 2831 (s), 2364 (w), 2343 (s), 2129 (w), 1606 (s), 1529 (s) 1502 (s), 1460 (m), 1439 (s), 1381 (w), 1286 (w), 1247 (w), 1211 (w), 1173 (w), 1103 (w), 1034 (w), 937 (m), 827 (w), 800 (m), 764 (s), 719 (s), 590 (m), 528 (m). Anal. Calcd. for $C_{64}H_{60}Mo_4N_{12}O_8S_4$ (**3**): C, 46.95; H, 3.69; N, 10.27. Found: C, 46.84; H, 3.55; N, 10.12.

Preparation of [Mo_2(*cis*-DAniF)$_2$]$_2$($\mu_{1,3}$-NCSe)$_4$, 4. This compound was prepared similarly to **3**. To a mixture of [Mo_2(*cis*-DAniF)$_2$(NCCH$_3$)$_4$](BF$_4$)$_2$ (0.35 g, 0.33 mmol) and K(NCSe) (0.29 g, 2.0 mmol) was added ethanol (15 mL). Upon stirring at ambient temperature, a red precipitate gradually formed. This mixture was stirred overnight; the supernatant solution was then decanted. After washing with ethanol (2 × 15 mL), the red solid was collected and dried overnight under a vacuum. A mixture of CH_2Cl_2/hexanes was used for crystallization. Red wedge-shaped crystals were produced after diffusion had proceeded for about four days. Yield: 0.26 g, 85%. ^{1}H NMR (in C_6D_6, ppm): 8.60 (s, 2H, N−C*H*−N), 8.43 (s, 2H, N−C*H*−N), 6.68 (d, 8H, aromatic), 6.50 (d, 8H, aromatic), 6.42 (d, 8H, aromatic), 6.34 (d, 8H, aromatic), 3.22 (s, 12H, OCH_3), 3.14 (s, 12H, OCH_3). UV−vis in CH_2Cl_2, λ_{max} (nm) (ε, M^{-1}cm^{-1}): 403 (5.5×10^3), 523 (7.3×10^3). IR (KBr, cm^{-1}): 2960 (m), 2831 (s), 2365 (w), 2345 (s), 2127 (w), 2058 (w), 1608 (s), 1533 (s) 1502 (s), 1460 (s), 1439 (s), 1383 (w), 1286 (w), 1246 (w), 1213 (w), 1174 (w), 1093 (w), 1032 (w), 937 (m), 824 (w), 800 (w), 764 (s), 590 (m), 528 (m). Anal. Calcd. for $C_{65.5}H_{63}Cl_3Mo_4N_{12}O_8Se_4$ (**4**·1.5CH_2Cl_2): C, 40.30; H, 3.25; N, 8.61. Found: C, 40.02; H, 3.26; N, 8.62.

X-Ray Structure Determinations. Data were collected on a Bruker SMART 1000 CCD area detector system. Cell parameters were determined using the program SMART.[38] Data reduction and integration were performed with the software SAINT.[39] Absorption corrections were applied by using the program SADABS.[40] The positions of the Mo atoms were found via direct methods using the program SHELXTL.[41] Subsequent cycles of least-squares refinement followed by difference Fourier syntheses revealed the positions of the remaining non-hydrogen atoms. Hydrogen atoms were added in idealized positions. All hydrogen atoms were included in the structure factor calculations. Additional details of data collection and refinement for **1**−**4** are given in Table 7. Crystallographic data are available as Supporting Information. All non-hydrogen atoms were refined with anisotropic displacement parameters. Electron density from disordered solvent molecules in **2**·PF_6 was squeezed using the program PLATON.[42] The core structures for **1**−**4** are presented in Figures 1 and 2. Selected bond distances and angles are listed in Tables 1 and 2.

Computational Details. Density functional theory[43] calculations were carried out using the hybrid Becke's[44] three-parameter exchange functional and the Lee−Yang−Parr[45] nonlocal correlation functional (B3LYP) in the Gaussian 03 program.[46] A double-ζ-quality basis set (D95)[47] was used for C, O, N, and

(38) *SMART for Windows NT*, version 5.618; Bruker Advanced X-ray Solutions, Inc.: Madison, WI, 2001.

(39) *SAINT*, version 6.36A; Bruker Advanced X-ray Solutions, Inc.: Madison, WI, 2002.

(40) *SADABS*, version 2.03; Bruker Advanced X-ray Solutions, Inc.: Madison, WI, 2002.

(41) Sheldrick, G. M. *SHELXTL*, version 6.10; Bruker Advanced X-ray Solutions, Inc.: Madison, WI, 2000.

(42) Spek, A. L. *PLATON - A Multipurpose Crystallographic Tool*; Utrecht University: The Netherlands, 2000.

(43) (a) Hohenberg, P.; Kohn, W. *Phys. Rev.* **1964**, *136*, B864. (b) Parr, R. G.; Yang, W. *Density-Functional Theory of Atoms and Molecules*; Oxford University Press: Oxford, 1989.

(44) (a) Becke, A. D. *Phys. Rev. A* **1988**, *38*, 3098. (b) Becke, A. D. *J. Chem. Phys.* **1993**, *98*, 1372. (c) Becke, A. D. *J. Chem. Phys.* **1993**, *98*, 5648.

(45) Lee, C. T.; Yang, W. T.; Parr, R. G. *Phys. Rev. B* **1998**, *37*, 785.

(46) Frisch, M. J.; Trucks, G. W.; Schlegel, H. B.; Scuseria, G. E.; Robb, M. A.; Cheeseman, J. R.; Montgomery, J. A., Jr.; Vreven, T.; Kudin, K. N.; Burant, J. C.; Millam, J. M.; Iyengar, S. S.; Tomasi, J.; Barone, V.; Mennucci, B.; Cossi, M.; Scalmani, G.; Rega, N.; Petersson, G. A.; Nakatsuji, H.; Hada, M.; Ehara, M.; Toyota, K.; Fukuda, R.; Hasegawa, J.; Ishida, M.; Nakajima, T.; Honda, Y.; Kitao, O.; Nakai, H.; Klene, M.; Li, X.; Knox, J. E.; Hratchian, H. P.; Cross, J. B.; Bakken, V.; Adamo, C.; Jaramillo, J.; Gomperts, R.; Stratmann, R. E.; Yazyev, O.; Austin, A. J.; Cammi, R.; Pomelli, C.; Ochterski, J. W.; Ayala, P. Y.; Morokuma, K.; Voth, G. A.; Salvador, P.; Dannenberg, J. J.; Zakrzewski, V. G.; Dapprich, S.; Daniels, A. D.; Strain, M. C.; Farkas, O.; Malick, D. K.; Rabuck, A. D.; Raghavachari, K.; Foresman, J. B.; Ortiz, J. V.; Cui, Q.; Baboul, A. G.; Clifford, S.; Cioslowski, J.; Stefanov, B. B.; Liu, G.; Liashenko, A.; Piskorz, P.; Komaromi, I.; Martin, R. L.; Fox, D. J.; Keith, T.; Al-Laham, M. A.; Peng, C. Y.; Nanayakkara, A.; Challacombe, M.; Gill, P. M. W.; Johnson, B.; Chen, W.; Wong, M. W.; Gonzalez, C.; Pople, J. A. *Gaussian 03*, revision C.02; Gaussian, Inc.: Wallingford, CT, 2004.

(47) Dunning, T. H.; Hay, P. J. In *Modern Theoretical Chemistry. 3. Methods of Electronic Structure Theory*; Schaefer, H. F., III, Ed.; Plenum Press: New York, 1977; pp 1−28.

(48) (a) Dunning, T. H. *J. Chem. Phys.* **1989**, *90*, 1007. (b) Woon, D. E.; Dunning, T. H. *J. Chem. Phys.* **1993**, *98*, 1358. (c) Wilson, A. K.; Woon, D. E.; Peterson, K. A.; Dunning, T. H. *J. Chem. Phys.* **1999**, *110*, 7667.

H atoms, as implemented in Gaussian. Correlation consistent double-ζ basis sets (CC-PVDZ)[48] were applied for the S and Se atoms. A small effective core potential representing the 1s2s2p3s3p3d core was used for the molybdenum atoms along with its corresponding double-ζ basis set (LANL2DZ).[49] All calculations were performed on either Origin 3800 64-processor SGI or Origin 2000 32-processor SGI supercomputers located at the Texas A&M supercomputing facility.

(49) (a) Wadt, W. R.; Hay, P. J. *J. Chem. Phys.* **1985**, *82*, 284. (b) Hay, P. J.; Wadt, W. R. *J. Chem. Phys.* **1985**, *82*, 299.

(50) (a) McGinnis, R. N.; Ryan, T. R.; McCarley, R. E. *J. Am. Chem. Soc.* **1978**, *100*, 7900. (b) Cotton, F. A.; Shang, M. *J. Cluster Sci.* **1991**, *2*, 121.

Acknowledgment. We thank the National Science Foundation (IR/D support) as well as the Robert A. Welch Foundation and Texas A&M University for financial support. We also thank Drs. Joseph H. Reibenspies and Shaoliang Zheng for helpful suggestions on crystallography. We are also grateful to the TAMU supercomputer facility and the Molecular Simulation Laboratory at TAMU for providing access to hardware and software.

Supporting Information Available: X-ray crystallographic data for **1**, **2**, **2**·PF_6, **3**·$3CH_2Cl_2$, and **4**·CH_2Cl_2 in standard CIF format. This material is available free of charge via the Internet at http://pubs.acs.org.